inorganics

MDPI

Article

Uranium-Mediated Thiourea/Urea Conversion on Chelating Ligands

Christelle Njiki Noufele [1], Maximilian Roca Jungfer [2], Adelheid Hagenbach [1], Hung Huy Nguyen [3] and Ulrich Abram [1,*]

[1] Institute of Chemistry and Biochemistry, Freie Universität Berlin, Fabeckstr. 34/36, D-14195 Berlin, Germany; chrisnjiki@gmail.com (C.N.N.); adelheid.hagenbach@uni-tuebingen.de (A.H.)
[2] Institute of Organic Chemistry, Ruprecht-Karls Universität Heidelberg, Im Neuenheimer Feld 270, D-69120 Heidelberg, Germany; maximilian.roca.jungfer@uni-heidelberg.de
[3] Department of Inorganic Chemistry, VNU University of Science, 19 Le Thanh Tong, Hanoi 100000, Vietnam; nguyenhunghuy@hus.edu.vn
* Correspondence: ulrich.abram@fu-berlin.de

Abstract: 2,6-Dipicolinoylbis(*N*,*N*-dialkylthioureas) and H_2L^{R2} react with uranyl salts and a supporting base (e.g., NEt_3) under formation of monomeric or oligomeric complexes of the compositions $[UO_2(L^{R2})(solv)]$ (solv = donor solvents) or $[\{UO_2(L^{R2})(\mu_2\text{-}OMe)\}_2]^{2-}$. In such complexes, the uranyl ions are commonly coordinated by the "hard" *O*,*N*,*O* or *N*,*N*,*N* donor atom sets of the central ligand unit and the lateral sulfur donor atoms remain uncoordinated. Their individual structures, however, depend on the reaction conditions, particularly on the equivalents of NEt_3 used. An unprecedented, selective hydrolysis of the uranium-coordinating bis(thioureato) ligands results in an *S*/*O* donor atom exchange at exclusively one thiourea side-arm, when an excess of NEt_3 is used. The resulting trimeric uranyl complexes are isolated in fair yields and have a composition of $[(UO_2)_3(L^{2Et2})_2(\mu_2\text{–}OR)(\mu_3\text{-}O)]^-$. H_2L^{2Et2} represents the newly formed 2,6-dipicolinoyl(*N*,*N*-diethylthiourea)(*N*,*N*-diethylurea) and R = H, Me, or Et. $\{L^{2Et2}\}^{2-}$ binds to the uranyl units via the pyridine ring, the dialkylurea arm, and the central carbonyl groups, while the thiourea unit remains uncoordinated. The central cores of the products consist of oxido-centered triangular $\{(UO_2)_3O\}^{4+}$ units. The observed reactivity is metal-driven and corresponds mechanistically most probably to a classical metal-catalyzed hydrodesulfurization. The hydrolytic thiourea/urea conversion is only observed in the presence of uranyl ions. The products were isolated in crystalline form and studied spectroscopically and by X-ray diffraction. The experimental findings are accompanied by DFT calculations, which help to understand the energetic implications in such systems.

Keywords: uranium; aroylthioureas; thiourea hydrolysis; synthesis; X-ray diffraction; DFT

Citation: Noufele, C.N.; Roca Jungfer, M.; Hagenbach, A.; Nguyen, H.H.; Abram, U. Uranium-Mediated Thiourea/Urea Conversion on Chelating Ligands. *Inorganics* **2024**, *12*, 295. https://doi.org/10.3390/inorganics12110295

Academic Editor: Wolfgang Linert

Received: 30 October 2024
Revised: 11 November 2024
Accepted: 14 November 2024
Published: 17 November 2024

1. Introduction

Uranyl ions, $\{UO_2\}^{2+}$, are regarded as "hard" metal ions with respect to Pearson's concept of hard and soft acids and bases [1]. Consequently, the coordination chemistry of uranium(VI) ions is dominated by complexes having predominantly "hard" donor atoms, frequently oxygen or nitrogen donor atoms [2–8]. Uranyl complexes with "soft" sulfur donor ligands are more rare. They are mainly restricted to compounds having chalcogenocarbamates, thiosemicarbazones and related compounds, bis(thiophosphinoyl)methanediides, or imidodiphosphinochalcogenides in their coordination sphere [9–17]. Such a situation is somewhat unsatisfactory, bearing in mind the increasing bioavailability of soluble uranium compounds, particularly in mining regions. The involved species are mainly uranyl complexes, and a deeper insight into their "biological" chemistry is required [18]. This also includes the formation of complexes with sulfur-containing ligands, which play a role in the uptake, the transport, and the storage of metal ions in biological systems. In recent years, a series of novel aspects of uranium chemistry entered the center of interest,

which also include practical applications in less-regarded areas such as catalysis, material science, or magnetochemistry [19–38]. This development requires more insights into the coordination chemistry of this actinide element with hitherto less-considered ligands.

While coordinated urea ligands are common for uranyl ions, and more than hundred structurally characterized examples can be found in the Cambridge structural database [39], representatives with simple thioureas and related ligands are extremely rare [40,41]. Recently, some reactions of uranyl compounds with the potentially chelating ligands shown in Figure 1 have been reported, together with the structural and ligand exchange chemistry of the products [42,43].

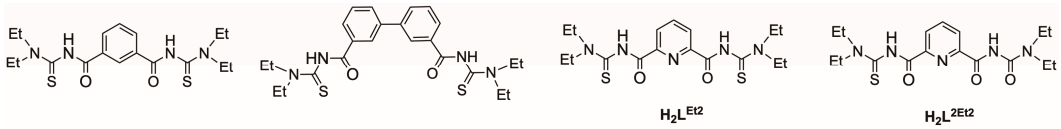

Figure 1. Potentially chelating thiourea ligands, which have been used for reactions with uranyl compounds [42,43].

In particular, the pyridine-centered ligand H_2L^{Et2} shows a versatile coordination chemistry with uranyl ions. It possesses a "medium soft" pyridine donor, two "hard" oxygen atoms, and two "soft" sulfur atoms. Accordingly, different coordination modes can be established with metal ions [42–49]. It could be shown that the "hard" $\{UO_2\}^{2+}$ ions prefer coordination with the central *O*,*N*,*O* or *O*,*N*,*N* donor atom sequences, but also products with coordinated sulfur atoms were isolated [42,43]. The coordination modes obtained with uranium, and observed so far, are summarized in Scheme 1.

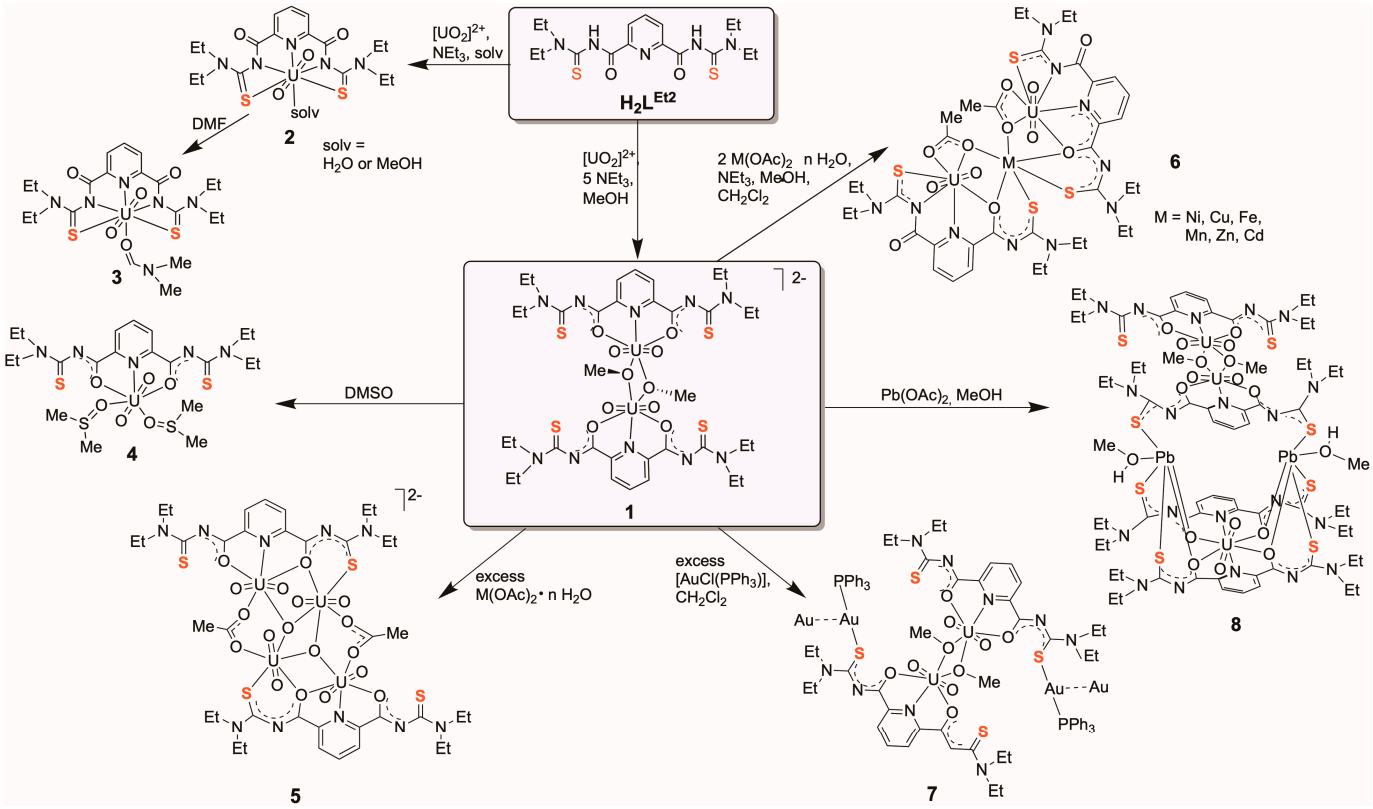

Scheme 1. Hitherto studied uranyl compounds obtained with H_2L^{Et2} ligands [42,43].

During the reactions of uranyl compounds with H_2L^{Et2}, it became evident that the nature of the isolated products is strongly dependent on the reaction conditions. In particular, the amount of supporting base was crucial for the composition of the obtained solids. The

labile, binuclear compound **1** plays a central role in such reactions. The methanolato bridges of this complex easily dissociate from uranium in solution and the resulting monomers form solvent complexes such as complex **4**, rearrange to oligomeric compounds such as compound **5**, or give bimetallic complexes (**6** to **8**), depending on the conditions applied. The sulfur atoms of the $\{L^{Et2}\}^{2-}$ ligands remain uncoordinated in most of the products or establish coordinative bonds to accompanying "soft" metal ions. An interesting reaction feature was found during the synthesis of the tetrameric compound **5**, in which two sulfur atoms bind to uranium. A careful inspection of the obtained single crystal X-ray structure showed that the thermal ellipsoids of the coordinated "sulfur atoms" were too large to justify a complete occupation with sulfur. Best results were obtained under the assumption that approximately 10 percent of these positions are occupied by oxygen [43]. This finding points to a (partial) hydrolysis of one of the thiourea functionalities upon prolonged reaction times in the presence of an excess of base, likely influenced by the metal ion. As a result, the non-symmetric ligand $\{L^{2Et2}\}^{2-}$ of Figure 1 has been formed. Stimulated by this unexpected result, we conducted ongoing reactions between compound **1** or other uranyl starting materials with H_2L^{Et2} using various amounts of the supporting base NEt_3.

2. Results and Discussion

2.1. $[(UO_2)_3(L^{2Et2})_2(\mu_2\text{-}OR)(\mu_3\text{-}O)]^-$ Complexes

2.1.1. Complex Formation and Spectroscopy

While reactions of common uranyl starting materials such as uranyl nitrate, uranyl acetate, or $(NBu_4)_2[UO_2Cl_4]$ with H_2L^{Et2}, and a slight excess (typically 5 equivalents) of triethylamin as a supporting base in methanol, give the dimeric, methanolato-bridged anion $[\{UO_2(L^{Et2})(\mu_2\text{-}OMe)\}_2]^{2-}$ (**1**) in good yields [42,43], similar reactions with a large excess of NEt_3 (25 equivalents or more) result in the hydrolysis of two of the thiourea units and the formation of trimeric complexes of the composition $[(UO_2)_3(L^{2Et2})_2(\mu_2\text{-}OR)(\mu_3\text{-}O)]^-$ (**9**–**11**). The connections between the uranium atoms are established by the carbonyl functionalities of the $\{L^{2Et2}\}^{2-}$ ligands, a central μ_3-bonded oxido ligand, and an OR^- unit, where the residue R represents H, Me, or Et depending on the synthetic route (see Scheme 2).

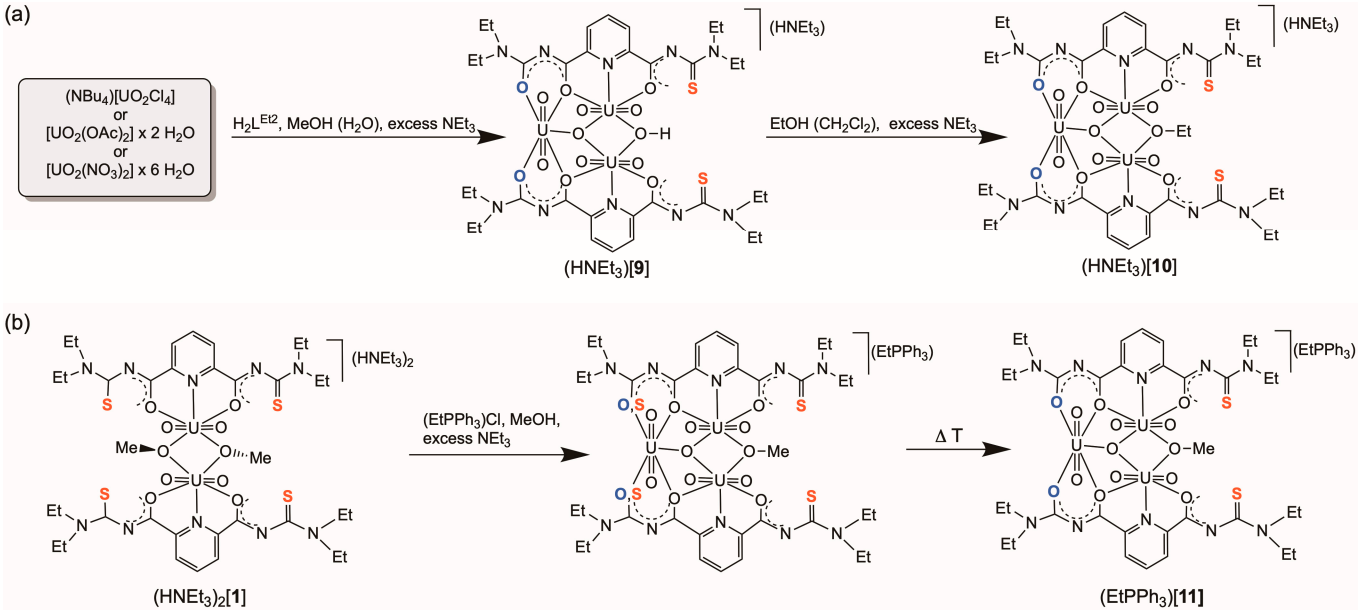

Scheme 2. Syntheses of $[(UO_2)_3(L^{2Et2})_2(\mu_2\text{-}OR)(\mu_3\text{-}O)]^-$ complexes (R = H: **9**, R = Et: **10**, R = Me:**11**) starting (**a**) from common uranyl salts and (**b**) starting from the dimeric complex $[\{UO_2(L^{Et2})(\mu_2\text{-}OMe)\}_2]^{2-}$.

The same type of complexes can be prepared starting from dimer **1** when it is exposed to an excess of NEt_3. The first evidence for such a route was found during a metathesis procedure in order to prepare the ethyltriphenylphosphonium salt of anion **1**. The desired $(EtPPh_3)_2[\{UO_2(L^{Et2})(\mu_2\text{-}OMe)\}_2]$ salt was indeed formed and could be isolated in crystalline form, when the amount of NEt_3, which was added for the stabilization of the anion, was limited to one or two equivalents [43], while using an excess of the base resulted in a subsequent "*S/O* exchange" in the $\{L^{Et2}\}^{2-}$ ligands and the formation of the trimeric anions containing the partially hydrolyzed ligand $\{L^{2Et2}\}^{2-}$.

The products can be isolated in good yields as air-stable, yellow solids by slow evaporation of the reaction mixtures. They are readily soluble in CH_2Cl_2 or DMSO, moderately soluble in $CHCl_3$, and almost insoluble in diethyl ether or hydrocarbons. Their IR spectra show the $\nu_{U=O}$ stretches at approximately 900 cm^{-1} and the $\nu_{C=O}$ vibrations appear around 1600 cm^{-1}, together with those of the amide and the pyridine fragments. The observed value corresponds to a bathochromic shift with regard to the stretch in the uncoordinated H_2L^{Et2} of approximately 80 cm^{-1} [50], which is somewhat less than in other chelates with this ligand, where the corresponding $\nu_{C=O}$ stretches appear at lower wavenumbers [42–49]. Nevertheless, it confirms the assumption of a considerable degree of electron delocalization within the chelate rings of the uranium complexes of the present study. The nature of the broad band at 1600 cm^{-1} as a superposition of $\nu_{C=C}$, $\nu_{C=N}$, and $\nu_{C=O}$ vibrations is supported by DFT considerations. A simulation of the corresponding is shown in the Supplementary Material. Broad bands at 3440 cm^{-1} are due to co-crystallized water and traces of water in the in KBr pellets. NH stretches could not be assigned, but they most probably appear together with the C-H vibrations around 3150 cm^{-1}.

In contrast with the dimeric complex $[\{UO_2(L^{Et2})(\mu_2\text{-}OMe)\}_2]^{2-}$, which readily dissociates in solution and forms monomeric $\{UO_2(L^{Et2})(\mu\text{-}OR)\}^-$ units (R = H, Me, Na), as could be shown in corresponding mass and NMR spectra [43], anions **9**, **10**, and **11** seem to be more stable. ESI(–) mass spectra taken from solutions of the corresponding salts confirm the presence of trimeric units. They do not dissociate in solution and can be transferred into the gas phase without decomposition. The only molecular position that was modified during such measurements is the bridging $\{OR\}^-$ unit, where a partial replacement of the hydroxo ligand in compound **9** by a methoxo unit was observed when the measurement was conducted in methanol. Figure 2a illustrates the molecular ion region of the corresponding mass spectrum. It is dominated by three ions, which can be assigned to the molecular anion $[(UO_2)_3(L^{2Et2})_2(\mu_2\text{–}OH)(\mu_3\text{-}O)]^-$ (calcd. m/z = 1997.4238), $[(UO_2)_3(L^{2Et2})_2(\mu_2\text{–}OMe)(\mu_3\text{-}O)]^-$ (calcd. m/z =1611.4395), and the cluster ion $[(UO_2)_3(L^{2Et2})_2(\mu_2\text{-}ONa)(\mu_3\text{-}O)]^-$ (calcd. m/z = 1619.4048), each with the correct isotopic patterns. Additionally, the spectrum gives evidence that the *S/O* exchange in two molecular positions is quantitative by the absence of peaks belonging to a complex with a residual $\{L^{Et2}\}^{2-}$ ligand, which would be expected at m/z = 1613.4010.

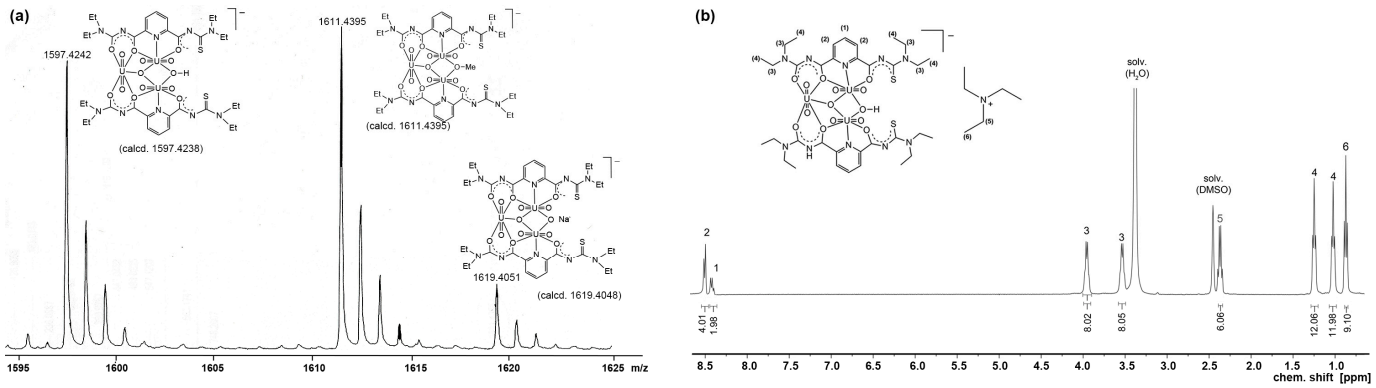

Figure 2. (**a**) Molecular ion region of the ESI(–) mass spectrum of $[(UO_2)_3(L^{2Et2})_2(\mu_2\text{-}OH)(\mu_3\text{-}O)]^-$ (**9**) in methanol and (**b**) ^1H NMR spectrum of the compound in DMSO-d_6.

The obvious stability of compound **9** in solution is supported by the NMR spectra of the compound. Figure 2b illustrates the ^{1}H NMR spectrum of **9** in DMSO-d_6 together with the assignment of the signals. In addition to the resonances of the ethyl groups of the triethylammonium cation, each two signals appear for the methyl and methylene groups of the organic ligands. The signals of the μ_2-hydroxido and the NH protons could not be observed under the conditions applied for the spectrum shown in Figure 2b or in $CDCl_3$. They are most probably not observed due to fast exchange processes. This is in accordance with the detection of an OH/OCH_3 exchange in the ESI(–) mass spectra in methanol (Figure 2a).

2.1.2. Single-Crystal X-Ray Crystallography

Yellow single crystals of $(HNEt_3)[(UO_2)_3(L^{2Et2})_2(\mu_2\text{-}OR)(\mu_3\text{-}O)]$ (R = H, Et) and $(EtPPh_3)[(UO_2)_3(L^{2Et2})_2(\mu_2\text{-}OMe)(\mu_3\text{-}O)]$ for X-ray diffraction were obtained by slow evaporation of CH_2Cl_2/alcohol solutions of the complexes. Ellipsoid representations of the complex anions are shown in Figure 3. The complex anions are composed of two $\{L^{2Et2}\}^{2-}$ ligands, three uranyl units, one μ_3-oxido ligand, and one $\{\mu_2\text{-}OR\}^-$ ligand (R = H, Me, Et), indicating a net charge of the complex of "−1". Both $\{L^{2Et2}\}^{2-}$ ligands each coordinate two uranyl ions in a tetradentate *O*,*O*,*N*,*O* fashion, while the two sulfur atoms remain uncoordinated. The three uranium atoms are connected to each other via a central μ_3-oxido ligand. Additionally, the atoms U2 and U3 are connected via a μ_2-hydroxido or -alkoxo ligand. This results in the formation of almost regular triangles of the uranium atoms, as is shown in Figure 3. The angles between the uranium atoms are between 56.9° and 65.6° and the U–U distances are between 3.714 and 3.919 Å; the individual values are depicted in Figure 3. All uranium ions are 7-coordinate and show a typical pentagonal-bipyramidal coordination environment. This is in contrast to the bonding situations in the few uranyl complexes with *S*-bonded thiourea units [40,41], where the metal ions have the coordination number "6". The uranyl bond lengths in complexes **9**, **10**, and **11** are unexceptional and range between 1.75 and 1.85 Å. Some selected bond lengths are summarized in Table 1. Details of the bond lengths and angles shall not be discussed here because of the limited data quality, which required the use of several restraints and constraints during the refinement procedures. More information is outlined in the Supplementary Material together with full lists of bond lengths and angles.

Table 1. Selected bond lengths (Å) in $(HNEt_3)[(UO_2)_3(L^{2Et2})_2(\mu_2\text{-}OH)(\mu_3\text{-}O)]$ ($(HNEt_3)$[**9**]), $(HNEt_3)[(UO_2)_3(L^{2Et2})_2(\mu_2\text{-}OEt)(\mu_3\text{-}O)]$ ($(HNEt_3)$[**10**]) and $(EtPPh_3)[(UO_2)_3(L^{2Et2})_2(\mu_2\text{-}OMe)(\mu_3\text{-}O)]$ ($(EtPPh_3)$[**11**]).

	U1–O1	**U1–O12**	**U1–O13**	**U1–O32**	**U1–O33**	**U2–O1**	**U2–O11**	**U2–N11**	**U2–O12**	**U2–O2**
9	2.196(9)	2.532(7)	2.340(8)	2.507(9)	2.308(8)	2.212(8)	2.345(8)	2.538(8)	2.481(8)	2.388(8)
10	2.205(15)	2.535(10)	2.342(10)	-	-	2.510(11)	2.341(11)	2.560(12)	2.535(10)	2.361(10)
11	2.202(5)	2.498(5)	2.342(5)	2.492(5)	2.331(6)	2.225(6)	2.351(5)	2.542(7)	2.504(5)	2.368(5)
	U3–O1	**U3–O31**	**U3–N31**	**U3–O32**	**U3–O2**	**C16–O11**	**C22–O12**	**C23–O13**	**C36–O31**	**C42–O32**
9	2.341(8)	2.316(8)	2.531(9)	2.486(8)	2.396(7)	1.28(1)	1.28(1)	1.26(1)	1.29(1)	1.31(1)
10	-	-	-	-	-	1.297(19)	1.290(18)	1.265(18)	-	-
11	2.227(6)	2.349(5)	2.542(6)	2.515(4)	2.349(5)	1.295(10)	1.286(9)	1.259(10)	1.286(9)	1.283(9)

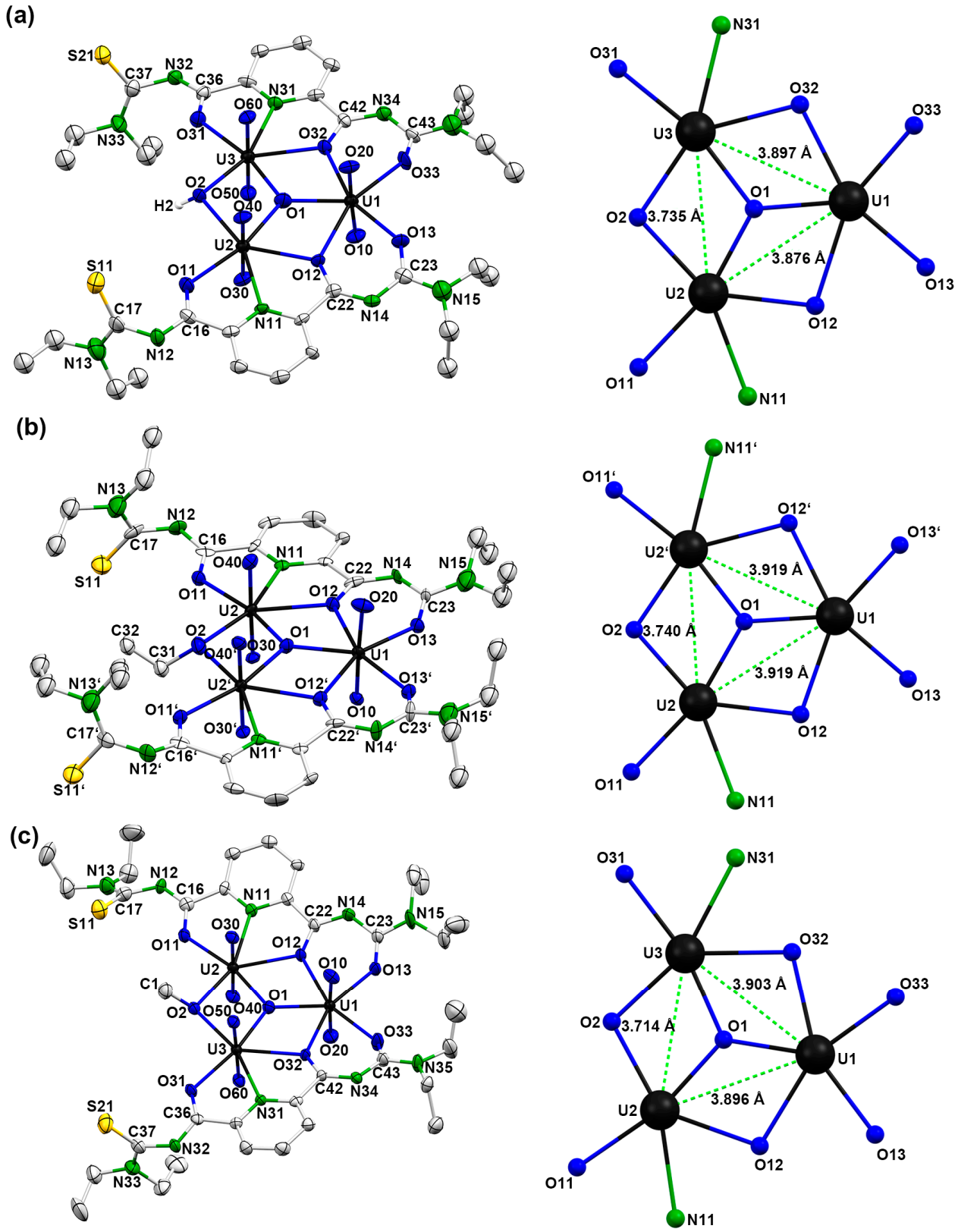

Figure 3. Ellipsoid representations of the complex anions of (**a**) $(HNEt_3)[(UO_2)_3(L^{2Et2})_2(\mu_2–OH)(\mu_3\text{-}O)]$ ((HNEt$_3$)[**9**]), (**b**) $(HNEt_3)[(UO_2)_3(L^{2Et2})_2(\mu_2–OEt)(\mu_3\text{-}O)]$ ((HNEt$_3$)[**10**]), and (**c**) $(EtPPh_3)[(UO_2)_3(L^{2Et2})_2(\mu_2–OMe)(\mu_3\text{-}O)]$ ((EtPPh$_3$)[**11**]), together with a visualization of the central cores formed by three uranyl units. Thermal ellipsoids represent 30 per cent probability. For color code see the atomic labeling scheme.

The uranium atoms U2 and U3 (or U2 and U2′ in complex **10**) are coordinated by two oxygen and the pyridine nitrogen atoms of each $\{L^{2Et2}\}^{2-}$ ligand. The third uranium atom, U1, is coordinated by the remaining two oxygen atoms of the $\{L^{2Et2}\}^{2-}$ ligands. The pentagonal bases of the uranyl bipyramids are completed by the central μ_3-oxygen atoms O1 and, in the case of U2 and U3, additionally by μ_2-bonded oxygen atom O2 of the $\{OR\}^-$ bridges. The formation of μ_3-bonded oxido ligands is a common feature in the structural chemistry of oligomeric and polymeric uranyl compounds and more than 150 examples can be found in the Cambridge structural database [39]. For molecules, which are composed of only three uranyl units, however, such a bonding situation is relatively rare [51–60]. The U–O bond lengths to the central oxido ligands found in these compounds range from 2.183 to 2.313 Å, which is in good agreement with the values obtained for the compounds of the present study. The U–O1 distances have values between 2.196(9) and 2.510(11) Å. Thus, they are shorter than those to the other equatorial oxygen donor atoms. Interestingly, the distances of the uranium atoms to the μ_2-oxygen atoms O12 and O32 are slightly longer than those to the mono-coordinated oxygen atoms of $\{L^{2Et2}\}^{2-}$ (O11, O13, O31, and O33). The pentagonal planes formed by the equatorial donor atoms and the uranium ions are almost perfectly planar and there are also only minor distortions between these planes within the trimeric complex anions. The largest distortion was found for complex 9 with a maximum deviation between two planes of 9.4°.

More information about the behavior of the trinuclear complex $(HNEt_3)[(UO_2)_3(L^{2Et2})_2(\mu_2\text{-}OEt)(\mu_3\text{-}O)]$ in solution was obtained by the analysis of the ESI(–) mass spectra of a solution of the complex in CH_2Cl_2/MeOH. Besides the peak of the molecular anion $[(UO_2)_3(L^{2Et2})_2(\mu_2\text{-}OEt)(\mu_3\text{-}O)]^-$, which is observed at m/z = 1627.4068, two fragments corresponding to the anions $[(UO_2)_3(L^{2Et2})_2(\mu_2\text{-}OMe)(\mu_3\text{-}O)]^-$ and $[(UO_2)_3(L^{2Et2})_2(\mu_2\text{-}OH)(\mu_3\text{-}O)]^-$ were detected at m/z = 1611.4307 and 1597.4153, respectively. This indicates the lability of the μ_2-bonded ligand, which can readily be replaced by related ligands, e.g., the solvent used for the measurement of NMR or mass spectra.

2.2. Hydrolysis of the Thiourea Units

The formation of complexes **9**, **10**, and **11** during reactions starting from the bis(thiourea) ligand H_2L^{Et2} or uranyl complexes thereof (see Scheme 2) requires a partial hydrolysis of thiourea functionalities of the starting material. Interestingly, the *S/O* exchange is observed exclusively at the ligand positions, which are used for the coordination of uranium, while the non-coordinating thiourea sulfur atoms remain untouched. Such a behavior strongly suggests a metal-mediated reaction, which finally results in a more stable (oxygen-coordinated) bonding situation around the "hard" uranyl Lewis acid. Since metal-driven or metal-mediated *S/O* exchange reactions in organic molecules are of general interest, e.g., for the industrial hydrodesulfurization processes of fossil fuels [61–66]. We conducted some additional experiments with the intention to understand some basic aspects of the observed reaction(s).

First, we studied the course of the reaction and could conclude that the addition of a sufficient amount (approximately 25-fold excess) of a supporting base is mandatory to start the hydrolytic reaction. With lower amounts of base, reactions between common uranyl starting materials and H_2L^{Et2} end with the formation of anionic $[\{UO_2(L^{Et2})(\mu\text{-}OMe)\}_2]^{2-}$ or neutral $[UO_2(L^{Et2})(solv)]$ complexes (solv = H_2O, MeOH or DMF) depending on the amount of base added [42,43]. In the monomeric $[UO_2(L^{Et2})(solv)]$ complexes, both sulfur atoms of the $\{L^{Et2}\}^{2-}$ ligands participate in the coordination of the uranyl ions and *S,N,N,N,S* chelates are established [42].

The intermediate coordination of sulfur atoms plays a role during the formation of the $\{L^{2Et2}\}^{2-}$ complexes of the present study. Spectroscopic and/or crystallographic evidence for such intermediate species has been found during the inspection of the reaction mixtures and/or by quenching the reaction after a few minutes by the precipitation of the product(s). An example is shown in Figure 4. It contains (a) an ESI(–) mass spectrum taken after 5 min from a reaction mixture between $(EtPPh_3)_2[\{UO_2(L^{Et2})(\mu_2\text{-}$

OMe)}$_2$] and NEt_3 in aqueous MeOH (see Scheme 2a) and (b) the result of an X-ray structure analysis taken from the material of such an (unfinished) reaction. The mass spectrum shows peaks at m/z = 1597.4153 ([$(UO_2)_3(L^{2Et2})_2(\mu_2$-OH)($\mu_3$-O)]$^-$, exchange product with water), m/z = 1611.4307 [$(UO_2)_3(L^{2Et2})_2(\mu_2$-OMe)($\mu_3$-O)]$^-$, molecular ion of the product), and m/z = 1627.4068, which can be assigned to an anion of the composition [$(UO_2)_3(L^{2Et2})(L^{Et2})(\mu_2$-OMe)($\mu_3$-O)]$^-$ (calcd. 1627.4068). Since mass spectrometry gives no direct information about the bonding situation inside the detected ions, the presence of a still-intact $\{L^{Et2}\}^{2-}$ ligand is not direct proof of the coordination of this ligand to uranium via a sulfur atom. Final evidence for this bonding mode, however, can be derived from a crystal structure determination on mixed $(EtPPh_3)[(UO_2)_3(L^{2Et2})_2(\mu_2$-OMe)($\mu_3$-O)]/$(EtPPh_3)[(UO_2)_3(L^{2Et2})(L^{Et2})(\mu_2$-OMe)($\mu_3$-O)] crystals. They were isolated by the precipitation of the product(s) from an incomplete reaction and contain approximately 10 percent of the complex with the sulfur-coordinated ligand $\{L^{Et2}\}^{2-}$. This can be derived from a corresponding refinement of the structural data, which results in thermal ellipsoids of reasonable quality, as can be seen in Figure 4b. The structure is very similar to that shown in Figure 3c, with the remarkable difference that the corresponding U–S and C–S bond lengths can be derived (U3–S13 2.583(17) Å, U3–O13 2.340(5) Å, C23–S13 1.709(18) Å, C23–O13 1.269(7) Å, U3–S33 2.568(18) Å, U3–O33 2.330(5), C43–S33 1.709(18) Å, C43–O33 1.261(8) Å).

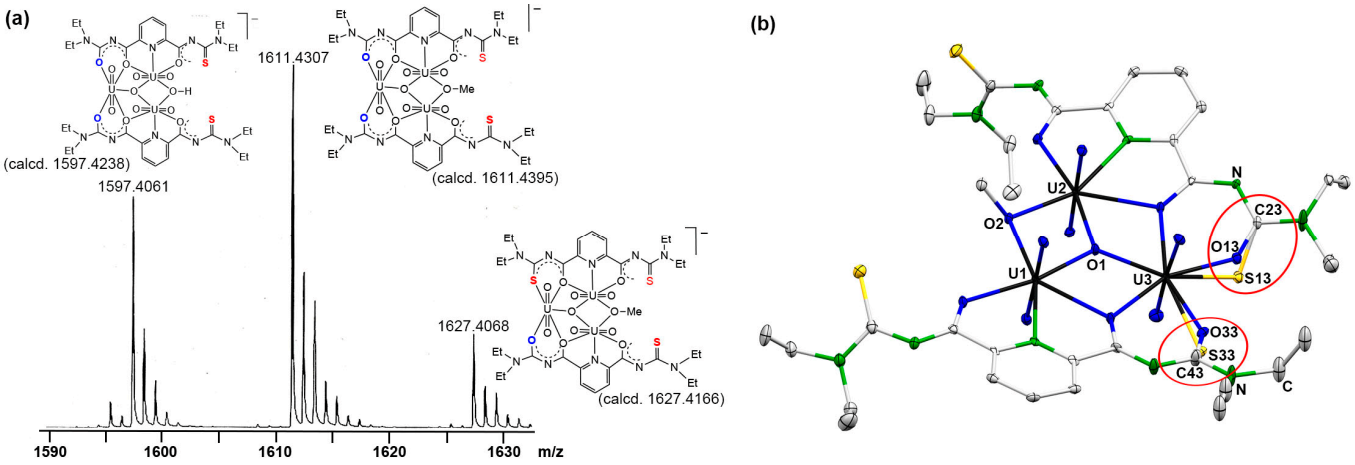

Figure 4. (**a**) ESI(–) mass spectrum of the (incomplete) reaction between $(EtPPh_3)_2$[{$UO_2(L^{Et2})(\mu_2$-OMe)}$_2$] and NEt_3 in aqueous MeOH and (**b**) ellipsoid representation of the complex anions of $(EtNPh_3)[(UO_2)_3(L^{2Et2})_2(\mu_2$–OH)($\mu_3$-O)] and $(EtNPh_3)[(UO_2)_3(L^{2Et2})(L^{Et2})(\mu_2$–OH)($\mu_3$-O)] derived from mixed crystals containing the two compounds in a ratio of 9:1 (see the atoms in the red circles). Thermal ellipsoids represent 30 per cent probability. For color code see atomic labelling scheme.

The detection of *S*-bonded uranyl units in the intermediates of the observed reaction suggests a mechanism for the hydrolysis of the thiourea units, in which the metal ions are involved. This has been experimentally proven by the treatment of H_2L^{Et2} in a mixture of CH_2Cl_2 and water at different pH values and the subsequent measurements of NMR spectra in the two phases. The results are illustrated in Figure 5, showing that the compound does not undergo decomposition in the pH range up to 14. It remains in the CH_2Cl_2 phase at low pH values until pH 9, and is deprotonated at higher pH values and extracts into the aqueous phase without decomposition.

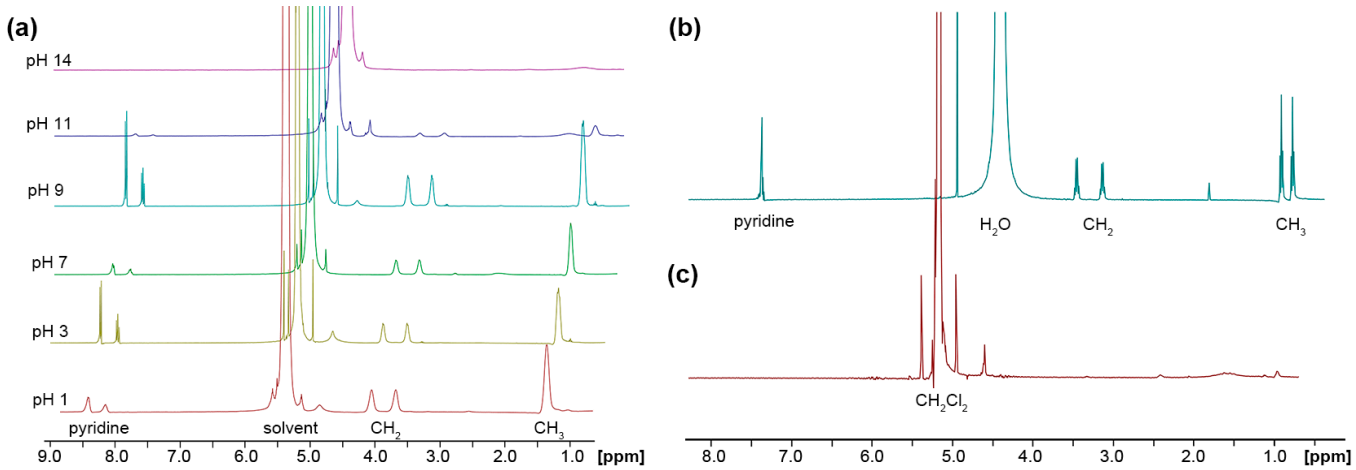

Figure 5. (**a**) ^{1}H NMR spectra recorded from the organic phase during the treatment of H_2L^{Et2} in a CH_2Cl_2/H_2O mixture at different pH values indicating an ongoing extraction into the aqueous phase at pH values > 9, (**b**) spectrum of the aqueous phases at pH 14 showing the presence of intact, deprotonated $\{L^{Et2}\}^{2-}$, and (**c**) the spectrum of the (almost empty) CH_2Cl_2 phase under the same conditions.

The mechanism of the uranium-mediated thiourea hydrolysis, and particularly the role of the "hard" uranyl ion, remains unclear. In previous studies about metal-driven thiourea hydrolysis, "soft" and thiophilic metal ions commonly found consideration, which readily form stable metal sulfides as the driving force of such reactions. A competent summary of attempts undertaken during the last century in this field and some new experiments with Cd^{2+} ions can be found in a recently published article [67]. Unfortunately, these experiments also did not give a clear picture of the mechanism and the role of potential intermediates, but conclusions have been drawn about the potential role of complex species.

In contrast to thiophilic metals, uranium compounds are not likely to drive thiourea hydrolysis via the formation of uranium sulfides. Instead, the formation of stable uranium–oxygen bonds could play a crucial role in the reaction mechanism. To explore this hypothesis, we undertook some DFT calculations for the *O*- and *S*-bonded uranium complexes, aiming to assess the energy differences between these species and their relative stabilities. It should be noted that similar reactions have not been observed before for the family of aroylthiourea ligands, which form complexes with a very large number of transition and post-transition metal ions [68–70]. To the best of our knowledge, there is only one related example with bis-*N*-isophthaloylselenourea, which is, as expected, much more susceptible to hydrolysis [71].

2.3. DFT Calculations

Calculations on the hypothetical, step-wise, gas-phase reaction between $[(UO_2)_3(L^{Et2})_2(\mu_2\text{-Me})(\mu_3\text{-O})]^-$ with one equivalent of H_2O to give $[(UO_2)_3(L^{2Et2})(L^{Et2})(\mu_2\text{-OMe})(\mu_3\text{-O})]^-$ and H_2S followed by the reaction with another equivalent of H_2O to give $[(UO_2)_3(L^{2Et2})_2(\mu_2\text{-OH})(\mu_3\text{-O})]^-$ and a second equivalent of H_2S were performed on the B3LYP/LANL2DZ(uranium)+6-311++G**(others) level in vacuum. There is a clear thermochemical preference for the uranium complexes containing the hydrolyzed ligand(s) in their coordination spheres (Scheme 3). The release of a free energy $\Delta(\Delta G)$ of approximately 70–80 kJ/mol per hydrolysis step is in accordance with the observed reactivity and product distribution observed in the conducted experiments.

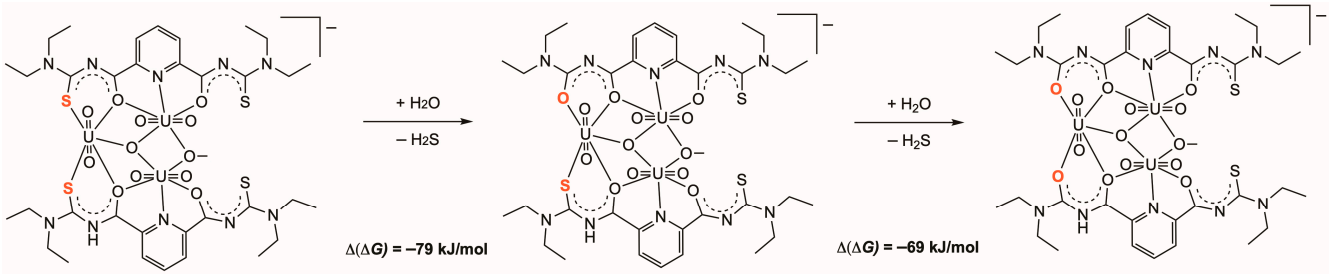

Scheme 3. DFT considerations relating to the stepwise hydrolytic reactions of the trimetallic uranium complex $[(UO_2)_3(L^{Et2})_2(\mu_2\text{–OMe})(\mu_3\text{-O})]^-$. Relative free energy differences for the reactions are provided in SI units (gas-phase, standard conditions, B3LYP/LANL2DZ(uranium)+6-311++G**(others) level).

Further calculations show that a total free energy preference $\Delta(\Delta G)$ is also obtained for the hydrolysis of the uncoordinated compound H_2L^{Et2}. The calculated energy $\Delta(\Delta G)$, however, is smaller, with ca. 50 kJ/mol for each individual hydrolysis step, but confirms a clear thermodynamic preference for the urea over the thiourea units in the uncoordinated compounds. With regard to the experimentally observed stability of the thiourea H_2L^{Et2} when exposed to water over a broad pH range, the results of the calculations strongly suggest that the pro-ligand is a kinetically stabilized, metastable molecule, which resists hydrolysis unless suitable catalysts such as $\{UO_2\}^{2+}$ ions enable this transformation by lowering the transition state energy. The calculation of a complete mechanism for the observed hydrolysis is beyond the scope of this paper and would additionally require the careful consideration of much smaller model systems as well as a dedicated Lewis-acid catalyst screening.

In search of a potential explanation for this large free energy difference, calculations on the same level of theory indicate a thermochemical free energy preference of the oxygen-coordinating isomer of $[(UO_2)_3(L^{2Et2})_2(\mu_2\text{–OMe})(\mu_3\text{-O})]^-$ over its analogous sulfur-coordinating isomer by roughly 70 kJ/mol, which is mainly driven by a difference in energy ΔE of ca. 65 kJ/mol (related calculations of the energy difference ΔE on the more accurate PBE0-GD3BJ/StuttgartRLC(uranium)+def2-TZVPPD(others) level are somewhat smaller with 42 kJ/mol). Therefore, the preference of hard Lewis acids such as uranyl ions for harder oxygen donors over softer sulfur donors may play a considerable role in this metal-enabled transformation, as predicted by the classical approach introduced by R. G. Pearson [1].

3. Materials and Methods

Unless otherwise stated, reagent-grade solvents and starting materials were used. Solvents were dried and distilled prior to use. H_2L^{Et2} was prepared according to a literature procedure [50].

3.1. Radiation Precaution

All synthetic work with uranium was performed in a laboratory approved for the handling of radioactive material. All personal working in this project were permanently monitored for potential contaminations.

3.2. Syntheses

$(HNEt_3)[(UO_2)_3(L^{2Et2})_2(\mu_2\text{–OH})(\mu_3\text{-O})]$. H_2L^{Et2} (79 mg, 0.2 mmol) was added to a stirred solution of $(NBu_4)_2[UO_2Cl_4]$ (90 mg, 0.1 mmol) in H_2O (3 mL). After 10 min, 5 drops of NEt_3 (ca. 65 mg, 2.5 mmol) were added and the reaction mixture was stirred at 50 °C for 1 h. A yellow solid precipitated during this time. It was filtered off, washed with diethyl ether, and dried in vacuum. Yellow needles suitable for X-ray diffraction were obtained after slow evaporation of a CH_2Cl_2 solution at room temperature. Yield: 68% (116 mg). IR (KBr, cm^{-1}): 3456(m), 3143(w), 3074(w), 2972(w), 2978(m), 2931(m), 1597(vs),

1492(s), 1425(s), 1373(vs), 1311(m), 1278(m), 1246(s), 1147(w), 1126(m), 1066(m), 1018(m), 902(vs), 769(m), 638(w). ^{1}H NMR ($(CD_3)_2SO$, ppm): 8.51 (d, 4H, *J* = 8.0 Hz, py); 8.41 (t, 2H, *J* = 8.0 Hz, py); 3.95 (q, 8H, *J* = 7.2 Hz, CH_2); 3.53 (q, 8H, *J* = 7.2 Hz, CH_2); 2.37 (q, 6H, *J* = 7.2 Hz, CH_2_$HNEt_3$); 1.25 (t, 12H, *J* = 7.2 Hz, CH_3); 1.02 (t, 12H, *J* = 7.2 Hz, CH_3); 0.87 (t, 9H, *J* = 7.2 Hz, CH_3_$HNEt_3$). ESI(–) MS (*m*/*z*: 1597.4242, $[M]^-$ (calcd. 1597.4238). UV/Vis (CH_2Cl_2, nm): 232 ($\varepsilon = 6.8 \times 10^3$ L mol^{-1} cm^{-1}), 264 ($\varepsilon = 2.0 \times 10^3$ L mol^{-1} cm^{-1}), 270 ($\varepsilon = 2.7 \times 10^3$ L mol^{-1} cm^{-1}), 277 ($\varepsilon = 1.8 \times 10^3$ L mol^{-1} cm^{-1}), 306 ($\varepsilon = 1.0 \times 10^3$ L mol^{-1}cm^{-1}), 368 ($\varepsilon = 0.2 \times 10^3$ L mol^{-1}cm^{-1}).

(EtPPh$_3$)[(UO$_2$)$_3$(L^{2Et2})$_2$(μ–OMe)(μ$_3$-O)]. A solution of ($EtPPh_3$)Cl (32.6 mg, 0.1 mmol) in MeOH (2 mL) containing 5 drops of NEt_3 (ca. 65 mg, 2.5 mmol) was added dropwise to a solution of the complex $(HNEt_3)_2[\{UO_2(L^{Et2})(\mu_2\text{-OMe})\}_2]$ (159 mg, 0.1 mmol) in CH_2Cl_2. (2 mL). The reaction mixture was evaporated slowly at room temperature. The resulting yellow crystals were collected, washed with MeOH, and dried under vacuum. They contained the products with incomplete S/O exchange. The reaction was completed by heating the reaction mixture for 1 h on reflux. Yield: 60% (114 mg). IR (KBr, cm^{-1}): 3433(m), 3055(w), 2968(w), 2926(m), 1593(vs), 1492(s), 1427(s), 1371(vs), 1246(s), 1111(m), 1008(m), 902(vs), 754(m), 688(m), 630(w). ^{1}H NMR ($(CD_3)_2SO$, ppm): 8.51 (d, 2H, *J* = 7.7 Hz, py); 8.43 (t, 1H, *J* = 7.7 Hz, py); 7.89–7.83 (m, 15H, Ph); 4.17–4.13 (m, 8H, CH_2); 3.97 (q, 4H, *J* = 7.2 Hz, CH_2,$EtPPh_3$); 3.62–3.52 (m, 8H, CH_2); 3.12 (s, 3H, OMe); 1.25 (t, 3H, *J* = 7.4 Hz, CH_3, $EtPPh_3$); 1.09–0.90 (m, 24H, *J* = 7.5 Hz, CH_3). ESI(–) MS (*m*/*z*: 1611.4395 $[M]^-$, (calcd. 1611.4395).

(HNEt$_3$)[(UO$_2$)$_3$(L^{2Et2})$_2$(μ–OEt)(μ$_3$-O)]. A solution of NEt_4Cl (32.6 mg, 0.1 mmol) in EtOH (2 mL) containing 5 drops of NEt_3 (ca. 65 mg, 2.5 mmol) was added dropwise to a solution of the dimeric complex $(HNEt_3)_2[\{UO_2(L^{Et2})_2(\mu\text{-OMe})\}_2]$ (159 mg, 0.1 mmol) in CH_2Cl_2 (2 mL). After heating for 1 h on reflux, the reaction mixture was evaporated slowly at room temperature. The obtained yellow crystals were collected, washed with EtOH, and dried under vacuum. Yield: 72% (126 mg). IR (KBr, cm^{-1}): 3442(w), 3078(w), 2978(w), 2934(w), 2874(w), 1597(vs), 1566(w), 1493(s), 1423(m), 1377(s), 1313(w), 1280(m), 1251(m), 1203(w), 1146(m), 1101(w), 995(m), 960(m), 904 (vs), 766(m), 696(w), 635(m). ^{1}H NMR ($(CD_3)_2SO$, ppm): 8.52 (d, 4H, *J* = 8.0 Hz, py); 8.37 (t, 2H, *J* = 8.0 Hz, py); 4.03–3.94 (m, 8H, CH_2); 3.57–3.52 (m, 8H, CH_2); 3.42–3.39 (m, 2H, *J* = 6.8 Hz, CH_2, OEt); 3.15 (q, 8H, *J* = 7.6 Hz, CH_2_$HNEt_3$); 1.26 (t, 3H, *J* = 6.8 Hz, CH_3, OEt); 1.13–1.07 (m, 24H, CH_3); 1.03 (t, 12H, *J* = 6.8 Hz, CH_3, $HNEt_3$). ESI(–) MS (*m*/*z*: 1625.4546 $[M]^-$ (calcd. 1625.4551).

3.3. Spectroscopic and Analytical Methods

IR spectra were measured as KBr pellets on a Shimadzu IR Affinity-1 (Shimadzu, Kyoto, Japan). The NMR spectra were recorded on JEOL ECS-400 or ECZ-400 400 MHz spectrometers (JEOL, Kyoto, Japan). ESI TOF mass spectra were measured with an Agilent 6210 ESI TOF (Agilent Technologies, Santa Clara, CA, USA. UV/vis spectra were measured and recorded on a SPECORD 40 instrument (Analytic Jena, Jena, Germany).

3.4. X-Ray Crystallography

The intensities for the X-ray determinations were collected on STOE IPDS-2T (STOE, Darmstadt, Germany) or Bruker CCD (BRUKER; Billerica, MA, USA) instruments with Mo/Kα radiation. The various temperatures applied are due to the experimental setup of the different diffractometers. Semi-empirical or numerical absorption corrections were carried out by the SADABS or X-RED32 programs [72,73]. Structure solution and refinement were performed with the SHELX programs [74,75] included in OLEX2, version 1.5 [76]. Hydrogen atoms were calculated for idealized positions and treated with the "riding model" option of SHELXL. The solvent mask option of OLEX2 was applied to treat diffuse electron density due to disordered solvent molecules where appropriate. Details are given in the Supplementary Materials. The representation of molecular structures was created using the program MERCURY, version 2024, 2.0 [77].

3.5. Computational Chemistry

DFT (Density Functional Theory) calculations were performed with the high-performance computing system of ZEDAT [78] using the program package GAUSSIAN 16 [79]. The gas-phase geometry optimizations were performed using coordinates derived from the X-ray crystal structures. Calculations were performed using the hybrid density functional B3LYP [80–82] together with the 6-311G basis set for all atoms as implemented in GAUSSIAN [83,84]. For initial optimization of uranium-containing compounds, the LANL2DZ basis set and the corresponding effective core potential (ECP) was used for uranium [85], while 6-311G was initially kept for the other atoms. The bigger 6-311++G** basis set was used for the other atoms to obtain more reliable geometries [83,84,86–88]. Relativistic, dispersion-corrected, all-electron calculations on the PBE0-DKH2-GD3BJ/SARC-DKH2(uranium)+aug-cc-pVTZ-DK(others) level as suggested in ref. [89] were attempted, but the system size proved prohibitive. For comparable accuracy, as outlined in ref. [90], calculations using the PBE0 hybrid functional ([91]) with Grimme dispersion and Becke–Johnson damping ([92]) using the Stuttgart relativistic large core ECP for uranium [93,94], and the def2-TZVPPD basis set for all other atoms [95,96], were attempted on the oxygen- and sulfur-bound isomers of $[(UO_2)_3(L^{2Et2})_2(\mu_2\text{-OH})(\mu_3\text{-O})]^-$ to verify the reliability of conclusions derived from the B3LYP thermochemistry. The thermochemistry of the hypothetical, step-wise hydrolysis of the free ligand $(L^{Et2})^{2-}$ to give $(L^{2Et2})^{2-}$ was calculated on the same level as the uranium complexes to ensure comparability of the results (using the 6-311++G** basis set [83,84,86–88] in frequency calculations based on the geometries obtained at the 6-311G level that have been reported before in ref. [43]). All basis sets were obtained from the EMSL database or the Basis Set Exchange repository [93,94]. Frequency calculations after the optimizations confirmed the convergence through the absence of imaginary frequencies.

4. Conclusions

Trinuclear uranyl complexes of the general composition $[(UO_2)_3(L^{2Et2})_2(\mu_2\text{-OR})(\mu_3\text{-O})]^-$ with partially hydrolyzed 2,6-dipicolinoylbis(*N*,*N*-diethylthiourea) ligands are formed from reactions of the ligand with common uranyl starting materials and an excess NEt_3. DFT calculations strongly suggest that the selective hydrolysis of one of the thiourea units is metal-mediated and the driving force for the observed reaction is the formation of the energetically favored uranium-oxygen bonds.

Supplementary Materials: The following supporting information can be downloaded at: https://www.mdpi.com/article/10.3390/inorganics12110295/s1, Table S1. Crystallographic data and data collection parameters. Figure S1. Ellipsoid representation of the structure of $(HNEt_3)$[**9**]. The thermal ellipsoids are set at a 30% probability level. Hydrogen atoms bonding to carbon atoms are omitted for clarity. Table S2. Bond lengths (Å) in $(HNEt_3)$[**9**]. Table S3. Bond angles (°) in $(HNEt_3)$[**9**]. Figure S2. Ellipsoid representation of the structure of $(HNEt_3)$[**10**], also illustrating the disordered parts of the counter ion. The thermal ellipsoids are set at a 30% probability level. Hydrogen atoms are omitted for clarity. Table S4. Bond lengths (Å) in $(HNEt_3)$[**10**]. Table S5. Bond angles (°) in $(HNEt_3)$[**10**]. Figure S3. Ellipsoid representation of the structure of $(EtPPh_3)$[**11**]. The thermal ellipsoids are set at a 30% probability level. Hydrogen atoms are omitted for clarity. Table S6. Bond lengths (Å) in $(EtPPh_3)$[**11**]. Table S7. Bond angles (°) in $(EtPPh_3)$[**11**]. Figure S4. Ellipsoid representation of the complexes contained in the $(EtPPh_3)[(UO_2)_3(L^{2Et2})_2(\mu_2\text{–OMe})(\mu_3\text{-O})]_{0.9}/[(UO_2)_3(L^{Et2})_2(\mu_2\text{–OMe})(\mu_3\text{-O})]_{0.1}$ mixed-crystals. The thermal ellipsoids are set at a 30% probability level. Hydrogen atoms are omitted for clarity. Table S8. Bond lengths (Å) in $(EtPPh_3)[(UO_2)_3(L^{2Et2})_2(\mu_2\text{–OMe})(\mu_3\text{-O})]_{0.9}/[(UO_2)_3(L^{Et2})_2(\mu_2\text{–OMe})(\mu_3\text{-O})]_{0.1}$. Table S9. Bond angles (°) in $(EtPPh_3)[(UO_2)_3(L^{2Et2})_2(\mu_2\text{–OMe})(\mu_3\text{-O})]_{0.9}/[(UO_2)_3(L^{Et2})_2(\mu_2\text{–OMe})(\mu_3\text{-O})]_{0.1}$. Figure S5. IR spectrum (KBr) of $(HNEt_3)[(UO_2)_3(L^{2Et2})_2(\mu_2\text{–OH})(\mu_3\text{-O})]$, $(HNEt_3)$[**9**]. Figure S6. ^{1}H NMR spectra of $(HNEt_3)[(UO_2)_3(L^{2Et2})_2(\mu_2\text{–OH})(\mu_3\text{-O})]$, $(HNEt_3)$[**9**], in DMSO-D_6. Figure S7. ^{1}H NMR spectra of $(HNEt_3)[(UO_2)_3(L^{2Et2})_2(\mu_2\text{–OH})(\mu_3\text{-O})]$, $(HNEt_3)$[**9**], in $CDCl_3$. Figure S8. ESI(–) mass spectrum of $(HNEt_3)[(UO_2)_3(L^{2Et2})_2(\mu_2\text{–OH})(\mu_3\text{-O})]$, $(HNEt_3)$[**9**], in CH_2Cl_2. Figure S9. IR spectrum (KBr) of $(HNEt_3)[(UO_2)_3(L^{2Et2})_2(\mu_2\text{–OEt})(\mu_3\text{-O})]$, $(HNEt_3)$[**10**]. Figure S10. ^{1}H NMR spectra

of $(HNEt_3)[(UO_2)_3(L^{2Et2})_2(\mu_2\text{–}OEt)(\mu_3\text{-}O)]$, $(HNEt_3)$[**10**], in DMSO-D_6. Figure S11. ESI(–) mass spectrum of $(HNEt_3)[(UO_2)_3(L^{2Et2})_2(\mu_2\text{–}OEt)(\mu_3\text{-}O)]$, $(HNEt_3)$[**10**], in CH_2Cl_2. Figure S12. IR spectrum (KBr) of $(EtPPh_3)[(UO_2)_3(L^{2Et2})_2(\mu_2\text{–}OMe)(\mu_3\text{-}O)]$, $(EtPPh_3)$[**11**]. Figure S13. ^{1}H NMR spectra of $(EtPPh_3)[(UO_2)_3(L^{2Et2})_2(\mu_2\text{–}OMe)(\mu_3\text{-}O)]$, $(EtPPh_3)$[**11**], in DMSO-D_6. Figure S14. Considered hydrolysis reactions of trimetallic uranium complexes and the corresponding uncoordinated proligands. Relative free energy differences for reactions and the hypothetical isomerization from *O*,*O* coordination in **C** to *S*,*S* coordination in **C′** are provided in SI units (gas-phase, standard conditions, B3LYP/LANL2DZ(uranium)+6-311++G**(others) level). Geometries for the ligand structures were optimized at the B3LYP/6-311G level. Figure S15. DFT optimized structure of $\mathbf{A^L}$ (see Figure S14). Hydrogen atoms bonded to carbon atoms are omitted for clarity. B3LYP/6-311G level. Taken from ref [42]. Figure S16. DFT optimized structure of $\mathbf{B^L}$ (see Figure S14). Hydrogen atoms bonded to carbon atoms are omitted for clarity. B3LYP/6-311G level. Figure S17. DFT optimized structure of $\mathbf{C^L}$ (see Figure S14). Hydrogen atoms bonded to carbon atoms are omitted for clarity. B3LYP/6-311G level. Figure S18. DFT optimized structure of **A** (see Figure S14). Hydrogen atoms are omitted for clarity. B3LYP/LANL2DZ(uranium)+6-311++G**(others) level. Figure S19. DFT optimized structure of **B** (see Figure S14). Hydrogen atoms are omitted for clarity. B3LYP/LANL2DZ(uranium)+6-311++G**(others) level. Figure S20. DFT optimized structure of **C** (see Figure S14). Hydrogen atoms are omitted for clarity. B3LYP/LANL2DZ(uranium)+6-311++G**(others) level. Figure S21. DFT optimized structure of **C′** (see Figure S14). Hydrogen atoms are omitted for clarity. B3LYP/LANL2DZ(uranium)+6-311++G**(others) level. Table S10. Free energies ΔG obtained by the DFT calculations (gas-phase, standard conditions, B3LYP/LANL2DZ(uranium)+6-311++G**(others) level). Geometries for the ligand structures were optimized at the B3LYP/6-311G level. Table S11. Energies *E* obtained by the DFT calculations (gas-phase, top: PBE0-GD3BJ/StuttgartRLC(uranium)+def2-TZVPPD(others) level; bottom: B3LYP/LANL2DZ(uranium)+6-311++G**(others) level). Figure S22. DFT-simulated IR frequencies for the $[(UO_2)_3(L^{2Et2})_2(\mu_2\text{–}OMe)(\mu_3\text{-}O)]^-$ anion with spectral resolutions of (a) 2 cm^{-1}, (b) 20 cm^{-1} and (c) 30 cm^{-1}. Note that no cation was included in the calculation. Despite the fact that the simulation was conducted for the optimized gas-phase structure, a good agreement was obtained with the frequencies in the experimental spectrum (see Figure S12).

Author Contributions: Conceptualization, U.A. and C.N.N.; methodology, C.N.N., M.R.J., H.H.N. and A.H.; validation, C.N.N., M.R.J. and A.H.; formal analysis, C.N.N., H.H.N., M.R.J. and A.H.; investigation, C.N.N., M.R.J. and H.H.N.; resources, U.A.; data curation, C.N.N., M.R.J. and A.H.; writing—original draft preparation, U.A.; writing—review and editing, C.N.N., A.H., M.R.J. and H.H.N.; visualization, C.N.N., U.A. and M.R.J.; supervision, U.A.; project administration, U.A.; funding acquisition, U.A. All authors have read and agreed to the published version of the manuscript.

Funding: This research was funded by the Rosa-Luxemburg Foundation, Freie Universität Berlin and the Deutsche Forschungsgemeinschaft (Core Facility BIOSUPRAMOL).

Data Availability Statement: Data are contained within the article and Supplementary Materials.

Acknowledgments: We would like to acknowledge the assistance of the Core Facility BioSupraMol supported by the DFG.

Conflicts of Interest: The authors declare no conflicts of interest.

References

1. Pearson, R.G. Hard and Soft Acids and Bases. *J. Am. Chem. Soc.* **1963**, *85*, 3533–3539. [CrossRef]
2. Albrecht-Schmitt, T.E. (Ed.) *Organometallic and Coordination Chemistry of the Actinides*; Springer: Berlin/Heidelberg, Germany, 2008; Volume 127.
3. Teixeira Costa Peluzo, B.M.; Kraka, E. Uranium: The nuclear Fuel Cycle and Beyond. *Int. J. Mol. Sci.* **2022**, *23*, 4655. [CrossRef] [PubMed]
4. Parker, B.F.; Zhang, Z.; Rao, L.; Arnold, J. An overview and recent progress in the chemistry of uranium extraction from Seawater. *Dalton Trans.* **2018**, *47*, 639–644. [CrossRef]
5. Loiseau, T.; Mihalcea, I.; Henry, N.; Volkringer, C. The crystal chemistry of uranium carboxylates. *Coord. Chem. Rev.* **2015**, *266–267*, 69–109. [CrossRef]
6. Abraham, F.; Arab-Chapelet, B.; Rivenet, M.; Tamain, C.; Grandjean, S. Actinide Oxalates, solid state structures and applications. *Coord. Chem. Rev.* **2014**, *266–267*, 28–68. [CrossRef]

7. Hayes, C.; Leznoff, D.B. Actinide coordination and organometallic complexes with multidentate polyamide ligands. *Coord. Chem. Rev.* **2014**, *266–269*, 155–170. [CrossRef]
8. Burns, C.J.; Eisen, M.S. Organoactinide Chemistry: Synthesis and Characterization. In *The Chemistry of the Actinide and Transactinide Elements*; Morss, L.R., Edelstein, N.M., Fuge, J., Eds.; Springer: Berlin/Heidelberg, Germany, 2006; Volume 5.
9. Ephritikhine, M. Molecular Actinide Compounds with soft chalcogen ligands. *Coord. Chem. Rev.* **2016**, *319*, 35–62. [CrossRef]
10. Nief, F. Complexes containing bonds between group 3, lanthanide or actinide metals and non-first-row main group elements (excluding halogens). *Coord. Chem. Rev.* **1998**, *178–180*, 13–81. [CrossRef]
11. Casellato, U.; Vidali, M.; Vigato, P.A. Actinide complexes with chelating ligands containing sulfur and amidic nitrogen donor atoms. *Coord. Chem. Rev.* **1979**, *28*, 231–277. [CrossRef]
12. Abram, U.; Schulz Lang, E.; Bonfada, E. Thiosemicarbazonato Complexes of Uranium. *Z. Anorg. Allg. Chem.* **2002**, *628*, 1873–1878. [CrossRef]
13. Garcia Santos, I.; Abram, U. Synthesis and structures of dioxouranium complexes with 2-pyridineformamide thiosemicarbazones. *Inorg. Chem. Commun.* **2004**, *7*, 440–442. [CrossRef]
14. Gaunt, A.J.; Scott, B.L.; Neu, M.P. Homoleptic uranium(III) imidodiphosphinochalcogenides including the first structurally characterised molecular trivalent actinide–Se bond. *Chem. Commun.* **2005**, *25*, 3215–3217. [CrossRef]
15. Gaunt, A.J.; Reilly, S.D.; Enriquez, A.E.; Scott, B.L.; Ibers, J.A.; Sekar, P.; Ingram, K.I.M.; Kaltsoyannis, N.; Neu, M.P. Experimental and Theoretical Comparison of Actinide and Lanthanide Bonding in $M[N(EPR_2)_2]_3$ Complexes (M = U, Pu, La, Ce; E = S, Se, Te; R = Ph, iPr, H). *Inorg. Chem.* **2008**, *47*, 29–41. [CrossRef] [PubMed]
16. Gaunt, A.J.; Scott, B.L.; Neu, M.P. A Molecular Actinide–Tellurium Bond and Comparison of Bonding in $[M^{III}\{N(TePiPr_2)_2\}_3]$ (M = U, La). *Angew. Chem. Int. Ed.* **2006**, *45*, 1638–1641. [CrossRef] [PubMed]
17. Ingram, K.I.M.; Kaltsoyannis, N.; Gaunt, A.J.; Neu, M.P. Covalency in the f-element–chalcogen bond: Computational studies of $[M(N(EPH_2)_2)_3]$ (M = La, U, Pu; E = O, S, Se, Te). *J. Alloys Compd.* **2007**, *444–445*, 369–375. [CrossRef]
18. Katz, S.A. The Chemistry and Toxicology of Depleted Uranium. *Toxics* **2014**, *2*, 50–78. [CrossRef]
19. Meyer, K.; Hartline, D.R. From Chemical Curiosities and Trophy Molecules to Uranium-Based Catalysis: Development for Uranium Catalysis as a New Facet in Molecular Uranium Chemistry. *JACS Au* **2021**, *6*, 698–709.
20. King, D.M.; Liddle, S.T. Progress in molecular uranium-nitride chemistry. *Coord. Chem. Rev.* **2014**, *266–267*, 2–15. [CrossRef]
21. Hayton, T.W. Recent developments in actinide–ligand multiple bonding. *Chem. Commun.* **2013**, *49*, 2956–2973. [CrossRef]
22. Ephritikhine, M. Recent Advances in Organoactinide Chemistry As Exemplified by Cyclopentadienyl Compounds. *Organometallics* **2013**, *32*, 2464–2488. [CrossRef]
23. Liddle, S.T. The Renaissance of Non-Aqueous Uranium Chemistry. *Angew. Chem. Int. Ed.* **2015**, *54*, 8604–8646. [CrossRef] [PubMed]
24. Fox, A.R.; Bart, S.C.; Meyer, K.; Cummins, C.C. Towards uranium catalysts. *Nature* **2008**, *455*, 341–349. [CrossRef] [PubMed]
25. Moro, F.; Mills, D.P.; Liddle, S.T.; van Slageren, J. The Inherent Single-Molecule Magnet Character of Trivalent Uranium. *Angew. Chem. Int. Ed.* **2013**, *52*, 3430–3433. [CrossRef]
26. Liddle, S.T.; van Slageren, J. Improving f-element single molecule magnets. *Chem. Soc. Rev.* **2015**, *44*, 6655–6669. [CrossRef]
27. Gardner, B.M.; Liddle, S.T. Small-Molecule Activation at Uranium(III). *Eur. J. Inorg. Chem.* **2013**, *2013*, 3753–3770. [CrossRef]
28. Hohloch, S.; Garner, M.E.; Parker, B.F.; Arnold, J. New supporting ligands in actinide chemistry: Tetramethyltetraazaannulene complexes with thorium and uranium. *Dalton Trans.* **2017**, *46*, 13768–13782. [CrossRef]
29. Andrews, M.B.; Cahill, C.L. Uranyl bearing hybrid materials: Synthesis, speciation and solid state structures. *Chem. Rev.* **2013**, *113*, 1121–1136. [CrossRef] [PubMed]
30. Frisch, M.; Cahill, C.L. Synthesis, structure and fluorescent studies of novel uranium coordination polymers in the pyridine dicarboxylic acid system. *Dalton Trans.* **2006**, *39*, 4679–4690. [CrossRef] [PubMed]
31. Carter, K.P.; Kalaj, M.; Cahill, C.L. Harnessing uranyl oxo atoms via halogen bonding interactions in molecular uranyl materials featuring 2,5-diiodobenzoic acid and N-donor capping ligands. *Inorg. Chem. Front.* **2017**, *4*, 65–78. [CrossRef]
32. Lussier, A.J.; Lopez, R.A.K.; Burns, P.C. A Revised and Expanded Structure Hierarchy of Natural and Synthetic Hexavalent Uranium Compounds. *Can. Min.* **2016**, *54*, 177–283. [CrossRef]
33. Zhang, Z.; Senchyk, G.; Liu, Y.; Spano, T.; Szymanowski, J.; Burns, P. Porous uranium diphosphonate frameworks with trinuclear units template by organic ammonium hydrolyzed from amine solvents. *Inorg. Chem.* **2017**, *56*, 13249–13256. [CrossRef] [PubMed]
34. Qiu, J.; Spano, T.; Dembowski, M.; Kokot, A.; Szymanowski, J.; Burns, P.C. Sulfate-Centered Sodium-Icosahedron-Templated Uranyl Peroxide Phosphate Cages with Uranyl Bridged by μ-η^1:η^2 Peroxide. *Inorg. Chem.* **2016**, *56*, 1874–1880. [CrossRef] [PubMed]
35. Serezhkina, L.B.; Grigor'ev, M.S.; Shimin, N.A.; Klepov, V.V.; Sereszhkin, V.N. First uranyl methacrylate complexes: Synthesis and structure. *Russ. J. Inorg. Chem.* **2015**, *60*, 672–683. [CrossRef]
36. Serezhkina, L.B.; Vologzhanina, A.V.; Klepov, V.V.; Sereszhkin, V.N. Crystal Structure of $R[UO_2(CH_3COO)_3]$ ($R = NH_4^+$, K^+, or Cs^+). *Crystallogr. Rep.* **2010**, *55*, 773–779. [CrossRef]
37. Carter, K.P.; Kalaj, M.; Kerridge, A.; Ridenour, J.A.; Cahill, C. How to Bend the Uranyl Cation via Crystal Engineering. *Inorg. Chem.* **2018**, *57*, 2714–2723. [CrossRef]

38. Ridenour, J.A.; Cahill, C.L. Synthesis, structural analysis, and supramolecular assembly of a series of in situ generated uranyl-peroxide complexes with functionalized 2,2′-bipyridine and varied carboxylic acid ligands. *New J. Chem.* **2018**, *42*, 1816–1831. [CrossRef]
39. Cambridge Crystallographic Database, Vers. 5.45. Available online: https://www.ccdc.cam.ac.uk/solutions/software/csd/ (accessed on 9 October 2024).
40. Maria, L.; Santos, I.C.; Santos, I. Uranium(iii) complexes supported by hydrobis(mercaptoimidazolyl)borates: Synthesis and oxidation chemistry. *Dalton Trans.* **2016**, *47*, 10601–10612. [CrossRef]
41. Kelley, S.P.; Smetana, V.; Nuss, J.S.; Dixon, D.A.; Vasiliu, M.; Mudring, A.-V.; Rogers, R.D. Dehydration of $UO_2Cl_2 \cdot 3H_2O$ and $Nd(NO_3)_3 \cdot 6H_2O$ with a Soft Donor Ligand and Comparison of Their Interactions through X-ray Diffraction and Theoretical Investigation. *Inorg. Chem.* **2020**, *59*, 2861–2869. [CrossRef]
42. Noufele, C.N.; Hagenbach, A.; Abram, U. Uranyl Complexes with Aroylbis(*N,N*-dialkylthioureas. *Inorg. Chem.* **2018**, *57*, 12255–12269. [CrossRef]
43. Noufele, C.N.; Schulze, D.; Roca Jungfer, M.; Hagenbach, A.; Abram, U. Bimetallic uranium complexes with 2,6-dipicolinoylbis(*N,N*-dialkylthioureas). *Molecules* **2024**, *29*, 5001. [CrossRef]
44. Nguyen, H.H.; Jegathesh, J.J.; Takiden, A.; Hauenstein, D.; Pham, C.T.; Le, C.D.; Abram, U. 2,6-Dipicolinoylbis(*N,N*-dialkylthioureas) as versatile building blocks for oligo- and polynuclear architectures. *Dalton Trans.* **2016**, *45*, 10771–10779. [CrossRef]
45. Pham, C.T.; Nguyen, H.H.; Hagenbach, A.; Abram, U. Iron(III) Metallacryptand and Metallacryptate Assemblies Derived from Aroylbis(*N,N*-diethylthioureas). *Inorg. Chem.* **2017**, *56*, 11406–11416. [CrossRef] [PubMed]
46. Pham, C.T.; Roca Jungfer, M.; Abram, U. Indium(III) {2}-Metallacryptates Assembled from 2,6-Dipicolinoyl-bis(***N,N***-diethylthiourea. *New J. Chem.* **2020**, *44*, 3672–3680. [CrossRef]
47. Jesudas, J.J.; Pham, C.T.; Hagenbach, A.; Abram, U.; Nguyen, H.H. Trinuclear '$Co^{II}Ln^{III}Co^{II}$' Complexes (Ln = La, Ce, Nd, Sm, Gd, Dy, Er and Yb) with 2,6-Dipicolinoyl-bis(*N,N*-diethylthiourea)—Synthesis, Structures and Magnetism. *Inorg. Chem.* **2020**, *58*, 386–395. [CrossRef]
48. Sucena, S.F.; Demirer, T.I.; Baitullina, A.; Hagenbach, A.; Grewe, J.; Spreckelmeyer, S.; März, J.; Barkleit, A.; daSilva Maia, P.I.; Nguyen, H.H.; et al. Gold-based Coronands as Hosts for M^{3+} Metal Ions: Ring Size Matters. *Molecules* **2023**, *28*, 5421. [CrossRef] [PubMed]
49. Santos dos Santos, S.; Schwade, V.D.; Schulz Lang, E.; Pham, C.T.; Roca Jungfer, M.; Abram, U.; Nguyen, H.H. Organotellurium(II) and -(IV) Compounds with Picolinoylbis(thioureas): From Simple 1:1 Adducts to Multimetallic Aggregates. *Eur. J. Inorg. Chem.* **2024**, *27*, e202400344. [CrossRef]
50. Douglass, I.B.; Dains, F.B. Some Derivatives of Benzoyl and Furoyl Isothiocyanates and their Use in Synthesizing Heterocyclic Compounds. *J. Am. Chem. Soc.* **1934**, *56*, 719–721. [CrossRef]
51. Lintvedt, R.L.; Heeg, M.J.; Ahmad, N.; Glick, M.D. Uranyl complexes of beta-polyketonates. Crystal and molecular structure of a mononuclear uranyl 1,3,5-triketonate and a novel trinuclear uranyl 1,3,5-triketonate with a trigonal-planar bridging oxide. *Inorg. Chem.* **1982**, *21*, 2350–2356. [CrossRef]
52. Charpin, P.; Lance, M.; Nierlich, M.; Vigner, D.; Livet, J.; Musikas, C. Structures de complexes d'azoture d'uranyle et de tétraalkylammonium. (I) Triazoture d'uranyle et de tétraéthylammonium. (II) μ_3-oxo-azoture d'uranyle et de tétraméthylammonium. *Acta Cryst. C* **1986**, *42*, 1691–1694. [CrossRef]
53. Gatto, C.C.; Schulz Lang, E.; Kupfer, A.; Hagenbach, A.; Abram, U. Mono-, Di- and Trinuclear Dioxo Complexes of Uranium Containing Hydrazonato and Azomethine Ligands. *Z. Anorg. Allg. Chem.* **2004**, *630*, 1286–1295. [CrossRef]
54. Back, D.F.; Manzoni de Oliveira, G.; Schulz Lang, E. Reversible Transamination of Alanine with Pyridoxal (Vitamin B6) in the Presence of the UO_2^{2+} Ion: Synthesis and X-ray Characterization of $[(UO_2PmHpyr)_3(\mu_3\text{-}O)]Cl \cdot 3H_2O$ (PmHpyr = Pyridoxaminylpiruvate Anion). *Z. Anorg. Allg. Chem.* **2007**, *633*, 729–733. [CrossRef]
55. Vologzhanina, A.V.; Serezhkina, L.B.; Neklyudova, N.A.; Serezkhin, V.N. Synthesis and characterisation of a trinuclear uranyl complex: Crystal structure of $(CN_3H_6)_5[(UO_2)_3O(OH)_2(CH_3COO)(C_2O_4)_3]$. *Inorg. Chim. Acta* **2009**, *362*, 4921–4925. [CrossRef]
56. Rodriguez-Dieguez, A.; Mota, A.J.; Seco, J.M.; Palacios, M.A.; Romerosa, A.; Colacio, E. Influence of metal ions, coligands and reaction conditions on the structural versatility and properties of 5-pyrimidyl-tetrazolate containing complexes. *Dalton Trans.* **2009**, *43*, 9578–9586. [CrossRef]
57. Szabo, Z.; Furo, I.; Csöregh, I. Combinatorial Multinuclear NMR and X-ray Diffraction Studies of Uranium(VI)-Nucleotide Complexes. *J. Am. Chem. Soc.* **2005**, *127*, 15236–15247. [CrossRef] [PubMed]
58. Yoshimura, T.; Nakaguchi, M.; Morimoto, K. Synthesis, Structures, and Proton Self-Exchange Reaction of μ_3-Oxido/Hydroxido Bridged Trinuclear Uranyl(VI) Complexes with Tridentate Schiff-Base Ligands. *Inorg. Chem.* **2017**, *56*, 4057–4064. [CrossRef] [PubMed]
59. Schaper, G.; Wenzel, M.; Hennersdorf, F.; Lindoy, L.F.; Weigand, J.J. Saccharified Uranyl Ions: Self-Assembly of UO_2^{2+} into Trinuclear Anionic Complexes by the Coordination of Glucosamine-Derived Schiff Bases. *Chem.-Eur. J.* **2021**, *27*, 8484–8491. [CrossRef]
60. Lu, H.; Zheng, Z.; Qiu, J.; Qian, Y.; Wang, J.-Q.; Lin, J. Unveiling the new function of uranyl molecular clusters as fluorometric sensors for UV and X-ray dosimetry. *Dalton Trans.* **2022**, *51*, 3041–3045. [CrossRef]

61. Gangguly, T.; Chakraborty, A.B.; Majumdar, A. Transition Metal Mediated Hydrolysis of C-S Bonds: An Overview of a New Reaction Strategy. *Org. Inorg. Au* **2023**, *3*, 332–349. [CrossRef]
62. Jones, W.D.; Vivic, D.A.; Martin Chin, R.; Roache, J.H.; Myers, A.W. Homogeneous models of thiophene HDS reactions. Selectivity in thiophene C-S cleavage and thiophene reactions with dinuclear metal complexes. *Polyhedron* **1997**, *16*, 3115–3128. [CrossRef]
63. Angelici, R.J. An overview of modeling studies in HDS, HDN and HDO catalysis. *Polyhedron* **1997**, *16*, 3073–3088. [CrossRef]
64. Bianchini, C.; Meli, A. Hydrogenation, Hydrogenolysis, and Desulfurization of Thiophenes by Soluble Metal Complexes: Recent Achievements and Future Directions. *Acc. Chem. Res.* **1998**, *31*, 109–116. [CrossRef]
65. Duayne Whitehurst, D.; Isoda, T.; Mochida, I. Present State of the Art and Future Challenges in the Hydrodesulfurization of Polyaromatic Sulfur Compounds. In *Advanced Catalysis*; Eley, D.D., Haag, W.O., Gates, B., Knözinger, H., Eds.; Academic Press: Cambridge, MA, USA, 1998; Volume 42, pp. 345–471.
66. Brunet, S.; Mey, D.; Pérot, G.; Bouchy, C.; Diehl, F. On the hydrodesulfurization of FCC gasoline: A review. *Appl. Catal. A Gen.* **2005**, *278*, 143–172. [CrossRef]
67. Garcia-Valenzuela, J.A. Simple Thiourea Hydrolysis or Intermediate Complex Mechanism? Taking up the Formation of Metal Sulfides from Metal-Thiourea Alkaline Solutions. *Comments Inorg. Chem.* **2017**, *73*, 99–115. [CrossRef]
68. Beyer, L.; Hoyer, E.; Liebscher, J.; Hartmann, H. Komplexbildung mit N-Acyl-thioharnstoffen. *Z. Chem.* **1981**, *21*, 81–91. [CrossRef]
69. Beyer, L.; Hoyer, E.; Hennig, H.; Kirmse, R.; Hartmann, H.; Liebscher, J. Synthese und Charakterisierung neuartiger Übergangsmetall-chelate von 1,1-Dialkyl-3-benzoyl-thioharnstoffen. *J. Prakt. Chem.* **1975**, *317*, 829–839. [CrossRef]
70. Koch, K.R. New chemistry with old ligands: N-alkyl- and N, N-dialkyl-N′-acyl(aroyl)thioureas in co-ordination, analytical and process chemistry of the platinum group metals. *Coord. Chem. Rev.* **2001**, *216−217*, 473–488. [CrossRef]
71. Rodenstein, A.; Odendal, J.A.; Kirmse, R.; Koch, K.R. Synthesis and molecular structure of the first binuclear {(bis-*N*-isophthaloyl ureato)copper(II)pyridine}$_2$ complex derived from the {(bis-*N*-isophthaloyl-selenoureato)copper(II)}$_2$ complex by O for Se atom exchange. *Coord. Chem. Commun.* **2011**, *14*, 99–102. [CrossRef]
72. Sheldrick, G. *SADABS, Vers. 2014/5*; University of Göttingen: Göttingen, Germany, 2014.
73. Coppens, P. The Evaluation of Absorption and Extinction in Single-Crystal Structure Analysis. In *Crystallographic Computing*; Muksgaard: Copenhagen, Denmark, 1979.
74. Sheldrick, G.M. A short history of SHELX. *Acta Crystallogr.* **2008**, *A64*, 112–122. [CrossRef]
75. Sheldrick, G.M. Crystal structure refinement with SHELXL. *Acta Crystallogr.* **2015**, *C71*, 3–8.
76. Dolomanov, O.V.; Bourhis, L.J.; Gildea, R.J.; Howard, J.A.; Puschmann, H. OLEX2: A complete structure solution, refinement and analysis program. *J. Appl. Crystallogr.* **2009**, *42*, 339–341. [CrossRef]
77. Macrae, C.F.; Sovago, I.; Cottrell, S.J.; Galek, P.T.A.; McCabe, P.; Pidcock, E.; Platings, M.; Shields, G.P.; Stevens, J.S.; Towler, M. Mercury 4.0: From visualization to analysis, design and prediction. *J. Appl. Cryst.* **2020**, *53*, 226–235. [CrossRef]
78. Bennett, L.; Melchers, B.; Proppe, B. *High-Performance Computing at ZEDAT*; Freie Universität: Berlin, Germany, 2020. Available online: https://refubium.fu-berlin.de/handle/fub188/26993 (accessed on 24 October 2024).
79. Frisch, M.J.; Trucks, G.W.; Schlegel, H.B.; Scuseria, G.E.; Robb, M.A.; Cheeseman, J.R.; Scalmani, G.; Barone, V.; Petersson, G.A.; Nakatsuji, H.; et al. *Gaussian 16, Revision A.03*; Gaussian, Inc.: Wallingford, CT, USA, 2016.
80. Vosko, S.H.; Wilk, L.; Nusair, M. Accurate spin-dependent electron liquid correlation energies for local spin density calculations: A critical analysis. *Can. J. Phys.* **1980**, *58*, 1200–1211. [CrossRef]
81. Becke, A.D. Density-functional thermochemistry. III. The role of exact exchange. *J. Chem. Phys.* **1993**, *98*, 5648–5652. [CrossRef]
82. Lee, C.; Yang, W.; Parr, R.G. Development of the Colle-Salvetti correlation-energy formula into a functional of the electron density. *Phys. Rev. B* **1988**, *37*, 785–789. [CrossRef] [PubMed]
83. Krishnan, R.; Binkley, J.S.; Seeger, R.; Pople, J.A. Self-consistent molecular orbital methods. XX. A basis set for correlated wave functions. *J. Chem. Phys.* **1980**, *72*, 650–654. [CrossRef]
84. McLean, A.D.; Chandler, G.S. Contracted Gaussian basis sets for molecular calculations. I. Second row atoms, Z=11-18. *J. Chem. Phys.* **1980**, *72*, 5639–5648. [CrossRef]
85. Hay, P.J. Ab initio studies of excited states of polyatomic molecules including spin-orbit and multiplet effects: The electronic states of UF_6. *J. Chem. Phys.* **1983**, *79*, 5469–5482. [CrossRef]
86. Spitznagel, G.W.; Clark, T.; von Ragué Schleyer, P.; Hehre, W.J. An evaluation of the performance of diffuse function-augmented basis sets for second row elements, Na-Cl. *J. Comput. Chem.* **1987**, *8*, 1109–1116. [CrossRef]
87. Clark, T.; Chandrasekhar, J.; Spitznagel, G.W.; von Ragué Schleyer, P. Efficient diffuse function-augmented basis sets for anion calculations. III. The 3-21+G basis set for first-row elements, Li-F.. *J. Comput. Chem.* **1983**, *4*, 294–301. [CrossRef]
88. Francl, M.M.; Pietro, W.J.; Hehre, W.J.; Binkley, J.S.; Gordon, M.S.; DeFrees, D.J.; Pople, J.A. Self-consistent molecular orbital methods. XXIII. A polarization-type basis set for second-row elements. *J. Chem. Phys.* **1982**, *77*, 3654–3665. [CrossRef]
89. Pantazis, D.A.; Neese, F. All-Electron Scalar Relativistic Basis Sets for the Actinides. *J. Chem. Theory Comput.* **2011**, *7*, 677–684. [CrossRef]
90. Shamov, G.A.; Schreckenbach, G.; Vo, T.N. A Comparative Relativistic DFT and Ab Initio Study on the Structure and Thermodynamics of the Oxofluorides of Uranium(IV), (V) and (VI). *Chem. Eur. J.* **2007**, *13*, 4932–4947. [CrossRef] [PubMed]
91. Adamo, C.; Barone, V. Toward reliable density functional methods without adjustable parameters: The PBE0 model. *J. Chem. Phys.* **1999**, *110*, 6158–6170. [CrossRef]

92. Grimme, S.; Ehrlich, S.; Goerigk, L. Effect of the damping function in dispersion corrected density functional theory. *J. Comput. Chem.* **2011**, *32*, 1456–1465. [CrossRef]
93. Feller, D. The role of databases in support of computational chemistry calculations. *J. Comput. Chem.* **1996**, *17*, 1571–1586. [CrossRef]
94. Schuchardt, K.L.; Didier, B.T.; Elsethagen, T.; Sun, L.; Gurumoorthi, V.; Chase, J.; Li, J.; Windus, T.L. Basis Set Exchange: A Community Database for Computational Sciences. *J. Chem. Inf. Model.* **2007**, *47*, 1045–1052. [CrossRef]
95. Rappoport, D.; Furche, F. Property-optimized Gaussian basis sets for molecular response calculations. *J. Chem. Phys.* **2010**, *133*, 134105. [CrossRef]
96. Weigend, F.; Ahlrichs, R. Balanced basis sets of split valence, triple zeta valence and quadruple zeta valence quality for H to Rn: Design and assessment of accuracy. *Phys. Chem. Chem. Phys.* **2005**, *7*, 3297. [CrossRef]